Network-reconfiguration-aware Power Oscillation Damping Controller for Converter-interfaced Generator Based Power Plants

Njegos Jankovic, Javier Roldán-Pérez, *Senior Member*, *IEEE*, Milan Prodanovic, *Senior Member*, *IEEE*, Jon Are Suul, *Member*, *IEEE*, Salvatore D'Arco, and Luis Rouco, *Senior Member*, *IEEE*

***Abstract*—In recent years, transmission system operators have started requesting converter-interfaced generators (CIGs) to participate in grid services such as power oscillation damping (POD). As power systems are prone to topology changes because of connection and disconnection of generators and lines, one of the most important requirements in the design of POD controller is to account for these changes. This can be done by either adjusting the controller structure during the operation or applying a fixed structure designed to address changes in the system. The fixed structure is usually preferred by transmission system operators since it is easier to determine its impact on the system. In this paper, a design procedure is proposed for network-reconfiguration-aware POD controller with fixed structure for CIG-based power plants that considers network configurations with any one line disconnected. The design procedure is based on frequency-response techniques, so it is suitable for application in CIG-based power plants, even in cases when a detailed small-signal model of the system is not available. Designs of a POD controller for the damping of critical system modes can be obtained by using active power, reactive power, or both power components simultaneously. The application to the design of a POD controller for a CIG-based power plant connected to the IEEE 39-bus system is presented as an example. Simulations performed in MATLAB and SimPowerSystems are used to validate the proposed design procedure. The validation includes an analysis of system performance with changes considered in the proposed designed procedure. Also, the system performance under unconsidered changes is examined, covering variations in load and inertia values, as well as disconnection of synchronous generators.**

***Index Terms*—Converter-interfaced generator, transmission system, frequency response, network reconfiguration, power oscillation damping.**

Manuscript received: January 16, 2024; revised: May 1, 2024; accepted: December 30, 2024. Date of CrossCheck: December 30, 2024. Date of online publication: March 11, 2025.

This work was developed in the framework of the SOLARFLESS project (TED2021-132854A-I00) and REDESFUERTES project (PID2022-142416OB-I00), both funded by MICIU/AEI/10.13039/501100011033 and by the European Union, NextGenerationEU/PRTR.

N. Jankovic, J. Roldán-Pérez, and M. Prodanovic are with IMDEA Energy Institute, Madrid, Spain (e-mail: njegos.jankovic@imdea.org; javier.roldan@imdea.org; milan.prodanovic@imdea.org).

L. Rouco is with Comillas Pontifical University, Institute for Research in Technology (IIT), Madrid, Spain (e-mail: rouco@comillas.edu).

J. A. Suul and S. D'Arco are with SINTEF Energy, Trondheim, Norway (e-mail: Jon.A.Suul@sintef.no; salvatore.darco@sintef.no).

DOI: 10.35833/MPCE.2024.000057

I. Introduction

LOW-FREQUENCY oscillations are inherent phenomena in power systems and are mainly caused by interactions between synchronous generators (SGs) [1]. To address these issues, the control system of SGs might include a power system stabilizer (PSS) loop [2]. The PSS acts upon changes in the grid frequency and adjusts the voltage reference of the SG. This allows SGs to provide power oscillation damping (POD) action. However, the projected large-scale integration of converter-interfaced generator (CIG) based power plants introduces uncertainty with respect to POD services in future power systems. The basic control strategies of CIG for renewable energy plants do not provide POD functionality. This change in the operation paradigm deteriorates the stability properties of power systems [3]. Furthermore, as the percentage of CIG-based power plants increases, this issue becomes more relevant [4]. Thus, the current trend is that transmission system operators now request participation in POD services from newly commissioned CIG-based power plants [5], [6].

The initial proposal for providing POD services with CIG-based power plants is inspired by the operation principle of the PSS and used only reactive power [7]. However, recent proposals show that both active and reactive powers can be used for POD purposes [8], [9]. Furthermore, the combined action of both power components can further improve the damping action [10], although negative interactions between two control loops may occur [11]. Hence, wind power plants [12], PV power plants [9], and battery systems [13] can all contribute to the damping of critical system modes. However, changes in the system can lead to a shift in these modes. Such changes can be caused by loss of generation or demand elements, as well as by network reconfiguration. Thus, the design of a POD controller should consider the changes caused by changes under the operation conditions of the system.

One method is to design a POD controller that is capable of adjusting to network reconfiguration [14]. Several such proposals have been made and most of them utilize different aspects of the power system operation for adjusting the POD controller. For example, in [15], the POD controller parameters are updated based on the load forecast. Reference [16]

proposes a predictive POD controller to address changes in the network operation point. The uncertainty of the network operation is addressed in [17] by using a self-tuning POD controller that includes a neural network for estimating the power system behavior. Furthermore, the POD controller can adapt to modifications in the operation state of the network [18]. Adaptive POD controllers are also suitable for addressing uncertainties arising from the power system model [17] and for uncertainties caused by the primary energy generation, e. g., wind speed [19]. These proposals show that the damping factor of the critical eigenvalues can be improved by adjusting the POD controller parameters even under severe system variations. However, the newly calculated parameter values may not be precise due to the discrepancy between the models used in the design and the real system.

Another method is to design a POD controller so that it is resilient to changes in network configuration. To do so, a design based on eigen-structure assignment is proposed in [20] where the POD controller helps with damping critical modes under different operation conditions. In [21], the impact of changes under the system operation conditions is analyzed. A POD controller is designed to guarantee a certain damping ratio for all critical modes under a set of different operation conditions. The results show that a POD controller with a group of first- and second-order filters meets this objective. However, the design procedure relies on the power system model for the closed-loop stability verification.

In general, the POD controller characteristics depend on the optimization method used to select controller parameters. For instance, researchers have proposed the use of bat optimization [22], cuckoo search algorithm [23], and particle swarm optimization [24]. Although different, these options achieve similar performance indices [25]. Another option to damp oscillations is to use a fuzzy controller. For example, [26] proposes a fuzzy Takagi-Sugeno model that has less fuzzy rules compared with a standard fuzzy controller. However, this method requires knowledge of advanced tools to deal with fuzzy systems. In [27], a POD controller with a fixed second-order structure is presented that shows resilience against the changes in the system. To improve the system resilience, the POD controller can be designed using a deep reinforcement learning method [28] or by solving an optimization problem. In [29], the objective function considers the transient stability aspects as well. The same problem has also been addressed by considering both regional pole placement and $\mathcal{H}_2$ performance metrics [18]. These proposals show that the POD controller can contribute to the damping of critical modes under variations in the system, such as changes in the system operation point. Although the studied variations have an influence on dynamic properties, they do not include aspects such as a disconnection of system elements that can have important impacts on both the operation point and the system dynamics.

In this paper, a design procedure is proposed for the network-reconfiguration-aware POD controller (hereafter called the proposed POD controller) with fixed structure for CIG-based power plant that considers network configurations with any electrical line disconnected. There are two initial assumptions. First, it is assumed that the small-signal model of the power system is not available. Therefore, system frequency response is used to obtain relevant information. Second, the power system under study has poorly-damped low-frequency oscillations. Then, the objective is to design the proposed POD controller for a new CIG-based power plant to be connected to such a system. A small-signal model is used in this paper only to analyze and validate the performance of the proposed POD controller. Compared with previous methods for POD by CIG, the contributions presented in this paper can be summarized as:

1) The proposed POD controller for a CIG-based power plant utilizes both active and reactive powers for oscillation damping.

2) The design method proposed in this paper relies only on measured system frequency responses. Also, only information from local measurements is required for the proposed POD controller.

3) The impact of changes in the network topology on the system dynamics is studied. The results are used to design the proposed POD controller with a fixed structure that improves system frequency stability in the range of low-frequency oscillations for different network topologies.

4) An optimization problem is defined to calculate the number of lead-lag filters in the proposed POD controller and their time-constant values, with the objective to achieve desired phase of frequency response for the proposed POD controller.

5) The controller gain value is determined in an iterative procedure, addressing the impact of the proposed POD controller within and outside the frequency range of interest.

The IEEE 39-bus system is used to verify the performance of the proposed method to design the proposed POD controller. The test includes an analysis of the system performance for network reconfiguration. Furthermore, the performance is examined for changes that are not considered in the design procedure for the proposed POD controller, i. e., changes in the system inertia, loading level, and disconnection of generator. This method is well suited to design the proposed POD controllers when the control designer has a simulation model, but not a small-signal model, since it is based on frequency-response techniques.

II. System Overview and Methodology

A. System Description

Figure 1 shows the diagram of IEEE 39-bus system, CIG-based power plant, and control diagram of one converter. It can be divided into three main parts. In Fig. 1(a), an IEEE 39-bus system is formed by ten generators G_1-G_{10}. Each generator includes an SG with a governor, an exciter, and a PSS [30]. In this paper, two modifications are made. Firstly, the PSS of several generators are adjusted to reduce the damping of certain modes while keeping the system stable. Secondly, an additional point of connection (POC) is introduced at bus 29, as shown in Fig. 1(a), and used to connect a CIG-based power plant.

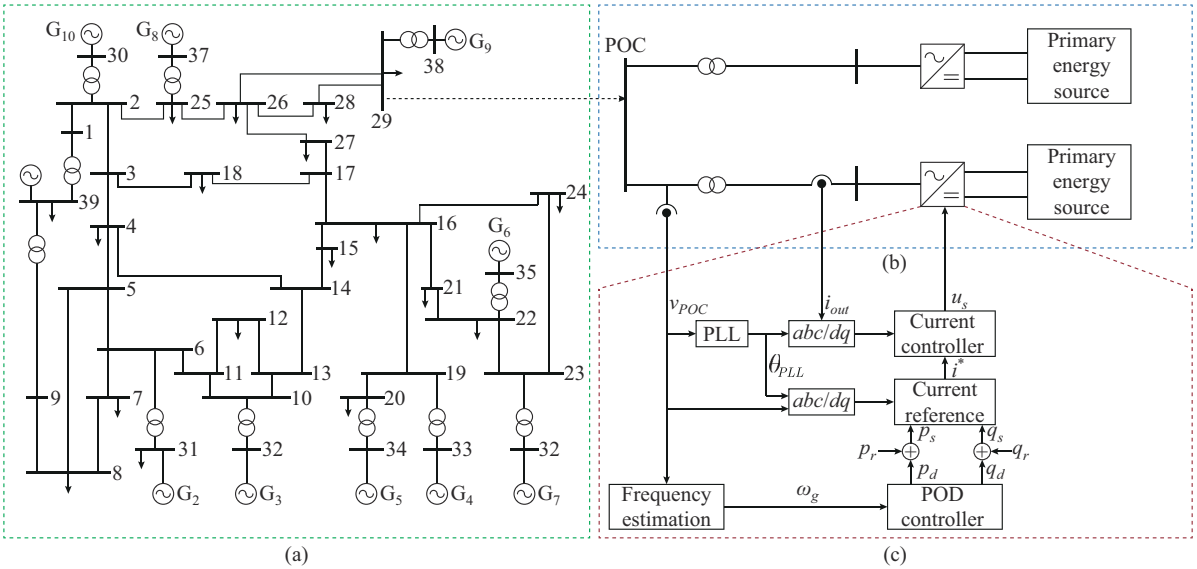

Fig. 1. Diagram of IEEE 39-bus system, CIG-based power plant, and control diagram of one converter. (a) IEEE 39-bus system. (b) CIG-based power plant. (c) Control diagram of one converter.

In Fig. 1(b), the electrical diagram of two additional CIGs are shown to represent the CIG-based power plant, which consists of two converters used to connect the primary energy sources to the network. These converters are connected to the POC via step-up transformers. The output current i_{out} and voltage v_{POC} are measured and used in the control algorithm.

Figure 1(c) shows an overview of the control diagram for one converter. First, the grid frequency ω_g is estimated from the measured voltage. Then, the proposed POD controller acts upon changes in the estimated frequency and produces active and reactive power references, i.e., p_d and q_d. The total active and reactive power references, i.e., p_s and q_s, are calculated by adding the controller references p_r and the references set by the system operator q_r. The power references are then converted to the references of the current controller i^* by considering v_{POC}. This calculation is done in a synchronous reference frame generated by a phase-locked loop (PLL) [31]. The angle estimated by the PLL is θ_{PLL}. Finally, the current controller defines the converter output voltage reference u_s.

B. POD Controller Structure

Figure 2 shows the block diagram of the proposed POD controller and power plant model. The power plant models in the active and reactive loops, i.e., $P_P(s)$ and $P_Q(s)$, represent the system dynamics from the active and reactive power references to the estimated network frequency. The proposed POD controller includes several elements, and its structure is inherited from the PSS controller structure [2]. The compensators $C_P(s)$ and $C_Q(s)$ consist of a series of lead-lag filters. Furthermore, band-pass filters, proportional gains, and saturation blocks are also included in the proposed POD controller. The symbol Δ refers to the signals of the linearised model. First, the band-pass filter $B(s)$ is acting upon deviations in the estimated ω_g. It removes components of ω_g outside the frequency range of interest. Then, the lead-lag filter compensates the open-loop phase of the plant in order to maximize the damping action of the proposed POD controller. p_c and q_c are the outputs of these controllers. The gains K_P and K_Q define the proportional action. Finally, the limiting actions of saturation blocks in the active and reactive powers, i.e., p_l and q_l, ensure that the capabilities of the power plant are not exceeded. This procedure produces p_d and q_d for POD from the studied POD control structure.

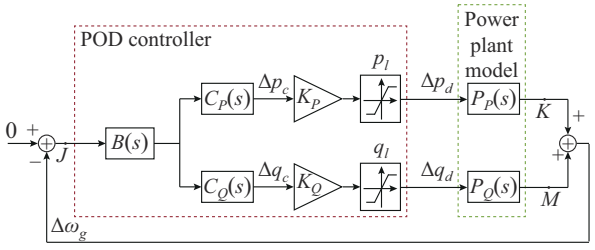

Fig. 2. Block diagram of proposed POD controller and power plant model.

C. Design Procedure of Proposed POD Controller

Figure 3 shows a flow diagram of the design procedure for the proposed POD controller, which is intended to be general and applicable to different networks, for cases where PODs with fixed parameters are preferred. In this paper, it is demonstrated using the IEEE 39-bus system as a case example. This design procedure is divided into three routines as follows.

1) Network Analysis

The network analysis is used to understand how the power plants $P_P(s)$ and $P_Q(s)$ change when the network is reconfigured. This routine is shown in Fig. 3(a). First, the set of modifications considered during the design procedure is defined. In this paper, modifications include the disconnection of each line in the original network topology, one by one. Also, it includes the nominal network configuration. This set of modifications can be extended to include cases such as

loss of generation units or loads in the network. Furthermore, the set of modifications can include changes under the network loading conditions or operation point. Such changes can emphasize nonlinear properties in the system. Thus, these changes can be used to study the system dynamic properties which might not be observed with changes in the network configuration. These cases will be used to test the performance of the proposed POD controller for changes which are not addressed during the design stage.

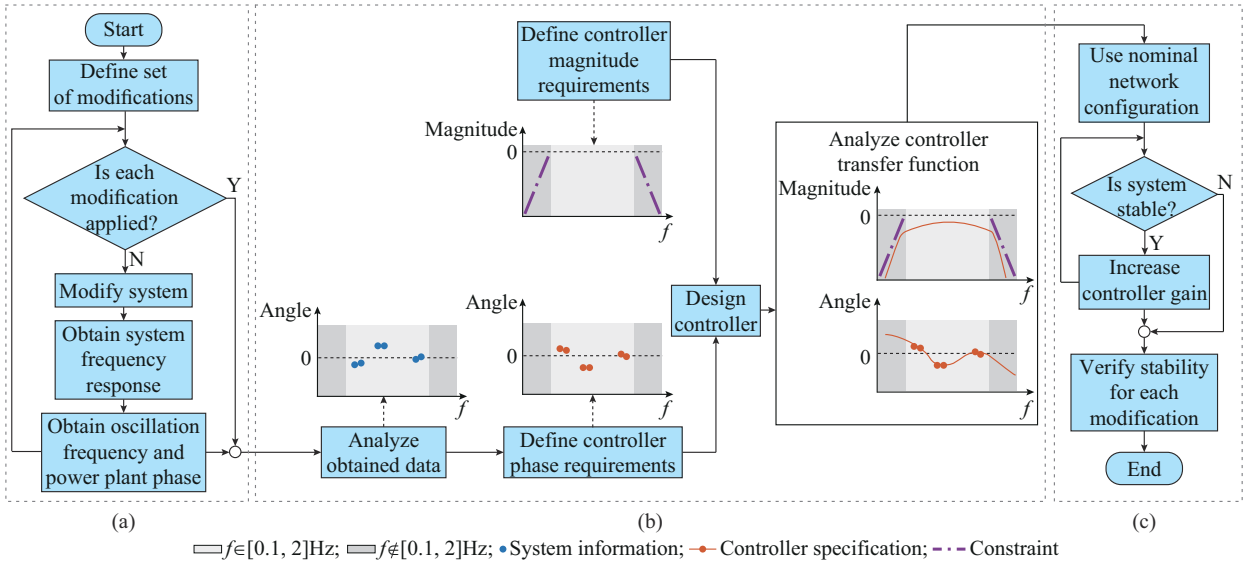

Fig. 3. Design procedure of proposed POD controller. (a) Network analysis. (b) Controller compensator design. (c) Design verification.

The next step in the power plant analysis is to obtain the frequency response of $P_P(s)$ and $P_Q(s)$ for each configuration. These transfer functions can be obtained from a detailed small-signal model. However, if small-signal models are not available, $P_P(s)$ and $P_Q(s)$ can be obtained by using system identification techniques [14]. Once these models are obtained, the peaks in the frequency response, i.e., resonance frequencies, are extracted. The phases at resonant frequencies, i.e., phases to be compensated by the proposed POD controller, are also calculated and stored. This procedure is repeated for each case in the given set of modifications.

Network equivalences are considered to reduce the required system information, which is beneficial for large systems and depends on additional details about the state and topology of the power system. Thus, further analysis based on network equivalences is considered outside the scope of this paper.

2) Controller Compensator Design

This routine includes the steps for designing the controller compensator, and is shown in Fig. 3(b). The compensators in the active and reactive power loops are designed separately, following the principle of superposition in control systems [14]. First, the information obtained in the previous routine is sorted and analyzed. In this step, the modifications that cause a significant change in the system dynamics, e.g., loss of lines connected to the power plant, are neglected. The remaining set of information is used to define the desired phase of frequency response for the proposed POD controller. In addition, two constraints are added to shape the magnitude of the frequency response. These constraints specify the maximum controller gain for the frequencies outside the frequency range of interest. This is of importance when the system frequency response is obtained by using the system identification method. In that case, the information about the system is determined by the characteristics of the perturbation signal, which is selected to obtain information within the frequency range of interest. Therefore, there is scarce information about the system dynamics outside the frequency range selected for the identification.

Finally, the controller compensator design is defined as an optimization problem in which the error between the specified and obtained phases is minimized. The constraints for the optimization problem are the aforementioned requirements for the magnitude. By solving the optimization problem, the proposed POD controller is inherently designed to contribute to the damping of low-frequency oscillations for a range of modifications.

3) Design Verification

The final routine for the design is shown in Fig. 3(c). First, the system frequency stability is examined for the nominal network configuration, i.e., all lines connected, with the proposed POD controller included. Then, the controller gains (K_P and K_Q) are incremented and the system response is obtained. If the system encounters instability or any other practical reason for limiting the controller gain, e.g., noise amplification, the iterative procedure is stopped. Finally, the system frequency stability is verified for all network configurations from the initial set of configurations. This procedure is conducted using the obtained system information before the proposed POD controller is implemented in CIG control algorithm. At this point, the final value of the proportional gain is determined. Then, during the system operation, the controller parameters remain fixed, even for changes in the

network topology.

III. Power Plant Analysis

During the system operation, the network topology changes every time when a line in the system is disconnected. Such changes have an important impact on the dynamic properties of the network. In [32], it has been shown that the change in the impedance of the lines affects the frequency of low-frequency modes. In terms of frequency response, those changes have a two-fold effect [14]. First, the changes in the frequency of critical modes are observed as changes in the oscillation frequency. This means that the peak in the magnitude of the frequency response occurs at different frequencies. The second effect is the change in the phase of the frequency response.

From Fig. 2, the frequency responses of $P_P(s)$ and $P_Q(s)$ can be defined as $P_P(\mathrm{j}\omega_{o,i})$ and $P_Q(\mathrm{j}\omega_{o,i})$.

$$P_P(\mathrm{j}\omega_{o,i}) = A_{P,i}\mathrm{e}^{\mathrm{j}\phi_{P,i}} \tag{1}$$

$$P_Q(\mathrm{j}\omega_{o,i}) = A_{Q,i}\mathrm{e}^{\mathrm{j}\phi_{Q,i}} \quad \omega_{o,i} \in \Omega, i \in I \tag{2}$$

where $\omega_{o,i}$ is the frequency of oscillations; $A_{P,i}$, $\phi_{P,i}$, and $\phi_{Q,i}$ are the magnitude and phases of the frequency response at $\omega_{o,i}$, respectively; I is the set of the number of oscillation frequencies; i is an element in the set I; and Ω is the set representing oscillation frequencies of interest. Then, the phases of the power plants at (1) and (2) are organized in corresponding sets as:

$$\Phi_{P,n} = \{\phi_{P,1}, \phi_{P,2}, ..., \phi_{P,i}\} \tag{3}$$

$$\Phi_{Q,n} = \{\phi_{Q,1}, \phi_{Q,2}, ..., \phi_{Q,i}\} \tag{4}$$

where $\Phi_{P,n}$ and $\Phi_{Q,n}$ are the sets calculated for each network configuration $\mathcal{N} = 1, 2, ..., N$, N is the number of cases considered, and n refers to an element in a given set of network configurations $\mathcal{N}$. Therefore, the set Ω_n should also bear the subscript n. Next, the information from all modifications is organized and grouped as:

$$\Omega = \{\Omega_1, \Omega_2, ..., \Omega_n\} \tag{5}$$

$$\Phi_P = \{\Phi_{P,1}, \Phi_{P,2}, ..., \Phi_{P,n}\} \tag{6}$$

$$\Phi_Q = \{\Phi_{Q,1}, \Phi_{Q,2}, ..., \Phi_{Q,n}\} \quad \forall n \in \mathcal{N} \tag{7}$$

where Φ_P and Φ_Q are the sets that contain phases for all the possible network configurations. To design the proposed POD controllers, the values in Φ_P and Φ_Q will also include the phase shift introduced by additional filters added in the loop.

If a power system model is not available, the information required for power plant analysis can be obtained by using system identification techniques [33]. In such a case, the system is perturbed by modifying the active and reactive power references and the system frequency response is measured. In this paper, the system frequency response is obtained using the Control System Design Toolbox of MATLAB [34] for simplicity.

IV. Design Method of Proposed POD Controller

A. Controller Element Definition

$B(s)$ is applied to attenuate the signal content outside the range of low-frequency oscillations $[0.1, 2]$Hz, which consists of high-pass and low-pass filters connected in series.

$$B(s) = \frac{s}{s + 1/T_h}\frac{1}{s/T_l + 1} \tag{8}$$

where T_h and T_l are the time constants of the high-pass and low-pass filters, respectively. The values of ω_h and ω_l are selected by considering the frequency range of low-frequency oscillations. Consequently, these cut-off frequencies need to be selected so that $B(s)$ attenuates the signal frequency content outside the range of low-frequency oscillations. At the same time, $B(s)$ will introduce an additional phase shift into the system. This phase shift is calculated at each frequency in Ω and added to the corresponding elements in Φ_P and Φ_Q. Therefore, it will be compensated by $C_P(s)$ and $C_Q(s)$.

Compensators $C_P(s)$ and $C_Q(s)$ consist of a set of lead-lag filters connected in series. $C_P(s)$ and $C_Q(s)$ have the same structure and their parameters are defined following the same procedure. Thus, in the rest of the document, the developments are presented only for $C_P(s)$ (for simplicity). $C_P(s)$ is defined as:

$$C_P(s) = \frac{1 + sT_1}{1 + sT_2}\frac{1 + sT_3}{1 + sT_4} \cdot ... \cdot \frac{1 + sT_{c-1}}{1 + sT_c} \tag{9}$$

where $T_1, T_2, ..., T_c$ are the compensator time constants, while the subscript c represents the number of time constants.

The order of the compensator (9) should be selected, and it depends on two requirements. First, the requirements for the phase of $C_P(\mathrm{j}\omega)$ are defined to compensate for a set of phases obtained in the power plant analysis. This set of phases includes a number of points with large phase differences across a narrow frequency range. Therefore, a low-order transfer function may lead to a large deviation between the required phase and the phase introduced by $C_P(\mathrm{j}\omega)$, where ω represents the imaginary part of the complex variable s in the Laplace domain. At the same time, the results achieved with very high-order transfer functions would not necessarily result in significantly improved design performance. Furthermore, higher-order transfer functions are typically difficult to implement in real time [35]. Thus, the order of $C_P(s)$ represents a compromise between these two considerations. Also, the final number of lead-lag filters is case specific, since the set of frequencies and required phases are different for each case.

The order of the compensator and compensator time constants are selected based on the design procedure for the proposed POD controller. An example of this procedure is presented in Section V.

B. Design Objective

The method used to design the proposed POD controllers is based on the phase compensation of the open-loop power plant at the frequency of interest [36]. The open-loop transfer function $G(s)$ is defined as a transfer function from

point J to point M, in Fig. 2. Analytically, the compensation objective can be written as:

$$\phi_G = 0 \tag{10}$$

$$G(\mathrm{j}\omega_o) = A_G \mathrm{e}^{\mathrm{j}\phi_G} \tag{11}$$

where ϕ_G and A_G are phase and magnitude of the frequency response of $G(s)$ at frequency ω_o, respectively. The design method provides a system damping that is close to the optimal value [37]. Also, as the design is based on open-loop characteristics, the calculation of the compensator parameters can be easily automatized.

Two open-loop transfer functions can be calculated from Fig. 2. These transfer functions represent the active and reactive power dynamics, i.e., $G_P(s)$ and $G_Q(s)$, which are defined from point J to points K and M in Fig. 2, respectively. In [37], it has been shown that the criteria from (10) can be met by setting phases to zero for the two open-loop functions separately:

$$\phi_{GP} = \phi_{GQ} = 0 \tag{12}$$

where ϕ_{GP} and ϕ_{GQ} are the phases of $G_P(\mathrm{j}\omega_o)$ and $G_Q(\mathrm{j}\omega_o)$, respectively.

To meet the objectives presented in (12), each of $C_P(s)$ and $C_Q(s)$ should compensate the phase of its corresponding open-loop system at the oscillation frequencies [37]. Considering multiple oscillation frequencies and changes caused by network reconfiguration, this criteria can be defined as (only the active power loop is shown):

$$\phi_{GP}^{i,n} = \phi_{CP}^{i,n} - \phi_P^{i,n} = 0 \quad \forall i \in I,\ \forall n \in \mathcal{N} \tag{13}$$

where $\phi_{CP}^{i,n}$ is the phase of $C_P(\mathrm{j}\omega)$; and $\phi_P^{i,n} \in \Phi_P$ is the element.

The criteria from (13) means that the controller $C_P(s)$ needs to compensate the phase of the corresponding system for all oscillation frequencies and all network configurations. Such requirements are too strict, mainly for two reasons. First, the requirements for the phase of $C_P(\mathrm{j}\omega)$ would include many points in a very narrow frequency range (0.1 Hz to 2 Hz). Second, the power plant models for different network configurations might have the same frequency of oscillation with different phases. Therefore, trying to fully compensate for the phase in all the cases is not a reasonable solution. Instead, an alternative function to design the compensator is proposed in the following part.

The design objective in this paper is focused on the disconnection of any one line at a time. Nonetheless, it can be extended for its application to a wider range of modifications. For example, if the requirement is to address the disconnection of any two lines in the system, the design objective would still be valid. Also, the disconnection of transformer units and other network elements could be included. However, the extension of the proposed method to cover those cases needs to consider two factors. The first factor would be the number of points in Ω, Φ_P, and Φ_Q, and therefore the number of requirements for the phase in (13). This could result in longer computational time to solve the optimization problem. The second factor would be the possible changes in the system operation point and the possible partitioning of the system, namely, the disconnection of any two lines at the time, and the disconnection of transformer units represent severe changes in the system operation. Therefore, the system performance should be analyzed for those cases and additional steps to design the proposed POD controller that might be needed. With certain adaptations, the general methodology presented in this paper could be extended to cover the above mentioned situations. Thus, such an extension of the work would be relevant and of interest for further research.

C. Definition of Optimization Problem

A cost function is defined based on the criteria in (13).

$$\min_x \sum_{i \in I, n \in \mathcal{N}} \left| \phi_{CP}^{i,n} - \phi_P^{i,n} \right|^m \tag{14}$$

$$x = \left\{ T_1, T_2, ..., T_c \right\} \tag{15}$$

where x is the set of parameters of the controller transfer function; and m is the parameter that defines the error cost, and its value depends on the complexity of the optimization problem. Namely, the change among elements $\phi_P^{i,n} \in \Phi_P$ can be different depending on the results of the power plant analysis. This change has a direct impact on the complexity of the problem in (14). Therefore, m is case specific. An increase in the value of m leads to higher penalty for large deviations. The value of m depends on two criteria. The first criteria is the allowed average error for the controller design. This error determines the performance of the designed controller in damping multiple modes in various network configurations. The second criteria is the maximum allowed error for any case. Thus, the value of m is a compromise between these two criteria. To achieve $\phi_{CP}^{i,n}$ at the oscillation frequencies, the cost function in (14) must be minimized. To achieve this, the optimization algorithm modifies the parameters of the controller transfer function.

D. Constraint

The solution of (14) defines the controller parameters based on the required phases in the frequency range of low-frequency oscillations. Nonetheless, once the controller is introduced into the system, it affects the rest of the frequencies outside this range. If not addressed, the controller may lead to unwanted interactions with other control layers.

To address this issue, constraints are added to the optimization problem. These constraints ensure that the controller impact outside the range of low-frequency oscillations is lower than or within this range, and are defined as:

$$c: \left| C_P(\mathrm{j}\omega_{out}) \right| \le 1 \quad \forall \omega_{out} \in \Omega_{out} \tag{16}$$

where Ω_{out} is a set of frequencies; and ω_{out} is the element of Ω_{out}.

$$\omega_{out} \notin [0.1, 2] 2\pi \text{ rad/s} \quad \forall \omega_{out} \in \Omega_{out} \tag{17}$$

The constraints in (16) limit the magnitude of $C_P(\mathrm{j}\omega)$. It is relevant to mention that the controller gain, i.e., the gain in the range of interest, will be tuned in the last step of the design procedure (with K_P).

Another set of constraints is linked with the set of unknown x in the optimization problem (14). Namely, the un-

knowns in this problem are controller parameters. Thus, constraints for those parameters are necessary to guarantee that the obtained $C_P(s)$ is stable. The constraints T_k are defined as:

$$T_k > 0 \quad \forall k \in \{2, 4, 6, ...\} \tag{18}$$

E. Controller Gain

The controller gains K_P and K_Q are determined based on the system frequency response and, if available, on transient simulations. This procedure consists of two parts. In the first part, the system is analyzed for the case when all the lines are connected. Gain values are changed incrementally and the closed-loop frequency response of the system is observed. The information from this analysis describes the impact of the gains on the margins both inside and outside the range of low-frequency oscillations. Such change results in the improved damping of low-frequency modes. After finishing this procedure, the different gain values are tested in simulation, and the one with the best performance is selected. A trade-off between amplification at frequencies outside the frequency band of interest and damping of the low-frequency modes should be selected.

The objective for the selection of the controller gains can be defined by using $G(s)$ and the error transfer function $E(s)$ [36]. First, $G(s)$ is the transfer function between points J and K in Fig. 2. Based on this, $E(s)$ is defined as $E(s) = 1/(1+G(s))$. Then, the frequency response of $E(s)$ at $\omega_{o,i}$ is defined as:

$$\left| E\left(\mathrm{j}\omega_{o,i}\right) \right| = \left| \frac{1}{1+G\left(\mathrm{j}\omega_{o,i}\right)} \right| \tag{19}$$

where $G\left(\mathrm{j}\omega_{o,i}\right) = A_G^i \mathrm{e}^{\mathrm{j}\phi_G^i}$. The open-loop phase ϕ_G^i is reduced by designing the lead-lag filters in the proposed POD controller. Then, $\left|1+G\left(\mathrm{j}\omega_{o,i}\right)\right|$ will be increased (and $E\left(\mathrm{j}\omega_{o,i}\right)$ will be decreased) if the controller gain is increased.

Nonetheless, after a certain point, the damping of one or more modes would decrease. Furthermore, as the gain increases, the impact of the proposed POD controller outside the frequency range of interest is changing. The change can be observed as a decrease in stability margins below and above the POD frequency range, depending on the system characteristics. Therefore, the gain value selection considers different aspects of the controller impact on system stability inside and outside the range of low-frequency oscillations.

The second part of the procedure includes the verification of the system stability with the gain value selected in the first step. Here, the system frequency stability in the range of low-frequency oscillations is verified for all the network configurations from the initial set of configurations using the selected gain value. For this purpose, the set of power plants for different network configurations can be used. The relevant information is obtained in Section III and no additional identification procedure is required. If the system is unstable for any of the given network configurations, the first step of the procedure for the gain value selection needs to be repeated and a different gain value should be selected.

F. Controller Limit

During transients, the converter is delivering active and reactive power for oscillation damping. Depending on the amplitude of the frequency deviation, p_s and q_s can exceed the converter capacity. Therefore, it is necessary to define p_l and q_l at the output of the proposed POD controller. These limits are changing over time based on the network operation point and available energy from the primary energy source. This means that in the case of a large disturbance, the power delivered by CIG would be limited. Then, the impact of the proposed POD controller on the low-frequency oscillation would be constrained. However, this limitation would appear only during certain periods of the transients, i.e., peaks of delivered power. Therefore, for simplicity, these limits are kept constant in this paper. More details can be found in [37].

V. Result

In this section, numerical results are presented. First, the power plant analysis is conducted and the requirements to design the proposed POD controller are defined. Then, the results from different stages of the proposed design method are analyzed. Finally, an analysis of the system eigenvalues is conducted. This type of analysis provides insights into the performance of the proposed POD controller across a diverse set of test scenarios. The small-signal model used for analysis is not utilized in the design procedure, since the starting assumption is that such a model is not available.

A. Power Plant Description and Analysis

The methods used to model the system and generate the network configurations are described in Supplementary Material A.

Figures 4 and 5 show the phases of $P_P(\mathrm{j}\omega)$ and $P_Q(\mathrm{j}\omega)$ for different network configurations, i.e., ϕ_{PP} and ϕ_{PQ}, respectively. In both cases, three clusters of points are formed, corresponding to three different ranges of oscillation frequencies. Changes in each cluster describe how network reconfiguration affects the interactions between different generators in the system.

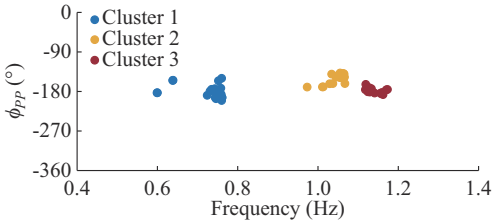

Fig. 4. Phase of $P_P(\mathrm{j}\omega)$ for different network configurations.

It can be observed that the angle and frequency variations differ between the clusters. ϕ_{PP} and ϕ_{PQ} vary around 90°, while the frequency of oscillations varies in the range of 0.1 Hz. The information used in power plant analysis is obtained from the system frequency response, which is obtained without reducing the order of the model.

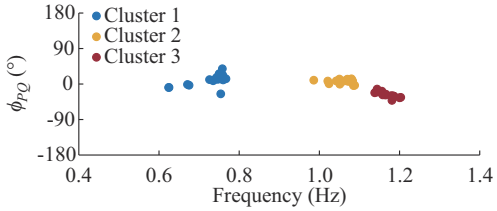

Fig. 5. Phase of $P_Q(\mathrm{j}\omega)$ for different network configurations.

B. Compensator Design

The compensators are designed according to the proposed method by using the information obtained from the power plant analysis. The optimization problem (14) with constraints from (16) is solved using *fmincon* function from MATLAB [34]. The optimization problem is solved on a desktop PC with Intel i5-8500 CPU and 8 GB RAM. The computational time required to design $C_P(s)$ and $C_Q(s)$ is 4.5 min and 3.4 min, respectively. The optimization problem (14) is solved when $m=3$. The compensator design accuracy is verified using the error $E_P^{i,n}$ between the specified and the obtained phase of $C_P(\mathrm{j}\omega)$ for all the elements in Ω.

$$E_P^{i,n}=\left|\phi_{CP}^{i,n}-\phi_P^{i,n}\right| \quad \forall i\in I,\ \forall n\in\mathcal{N} \tag{20}$$

$E_P^{i,n}$ corresponds to the individual elements of the sum that is used to define the cost function (14). Thus, by minimizing the cost function, $E_P^{i,n}$ is reduced. The error metric introduced at this stage is used for comparing different designs of the proposed POD controller. Therefore, other types of errors, e.g., least squares error, might be used.

Figures SB1 and SB2 of Supplementary Material B include the errors for both $C_P(s)$ and $C_Q(s)$.

In Table I, the mean and maximum errors for $C_P(s)$ and $C_Q(s)$, i.e., E_P and E_Q, are listed with different compensator orders. The compensator order is modified to examine the error and select the best-performing design for each power loop, independently.

TABLE I
MEAN AND MAXIMUM E_P AND E_Q WITH DIFFERENT COMPENSATOR ORDERS

Order	E_P (°)		E_Q (°)	
	Mean	Maximum	Mean	Maximum
1	164	179	17	41
2	15	27	17	41
3	14	27	17	41
4	14	27	16	38
5	15	39	16	38
6	14	27	16	38

For $C_P(s)$, it can be observed that the error is significantly reduced if a series of two lead-lag filters are used compared with using only one such filter. Further increase in the number of lead-lag filters leads to a reduced error, although the difference is not significant. Then, for $C_P(s)$ of order five, the maximum error increases significantly, while the compensator of order six gives the same results as those of order three and order four. In contrast, the error in $C_Q(s)$ does not change significantly when the order increases. By increasing the order from one to three, the error is not modified. Then, for order four to order six, the error is changed, although the improvement is not significant. These results show that the relation between the compensator order and the error is not linear. Therefore, the order of the compensator transfer function should be selected carefully upon determining the relation between the error and the compensator order. Based on the analysis, the orders for $C_P(s)$ and $C_Q(s)$ are set to be three and four, respectively. The compensator parameters can be found in Supplementary Material B.

Figure 6 shows the frequency response of $C_P(s)B(s)$ and magnitude of $B(\mathrm{j}\omega)$ for all elements in Ω_{out}. Figure 7 shows the frequency response of $C_Q(s)B(s)$ and magnitude of $B(\mathrm{j}\omega)$ for all elements in Ω_{out}. These figures show the combined frequency response of the band-pass filter and compensators in each loop, allowing to assess the total impact of the proposed POD controller on the system. It can be observed that the band-pass filter mainly determines the shape of the magnitude of the proposed POD controller, due to the magnitude constraints of $C_P(\mathrm{j}\omega)$ and $C_Q(\mathrm{j}\omega)$. Within the frequency range of interest, the magnitude of the proposed POD controller deviates from the band-pass filter. This is expected because in this frequency range the requirements for the phase of $C_P(\mathrm{j}\omega)$ and $C_Q(\mathrm{j}\omega)$ are specified and set.

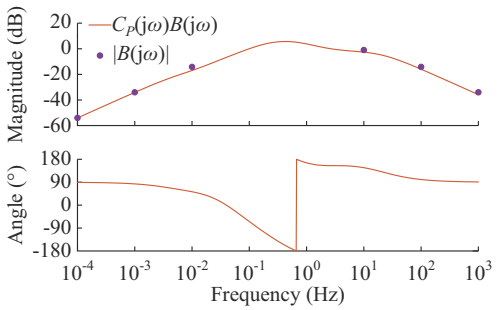

Fig. 6. Frequency response of $C_P(s)B(s)$ and magnitude of $B(\mathrm{j}\omega)$ for all elements in Ω_{out}.

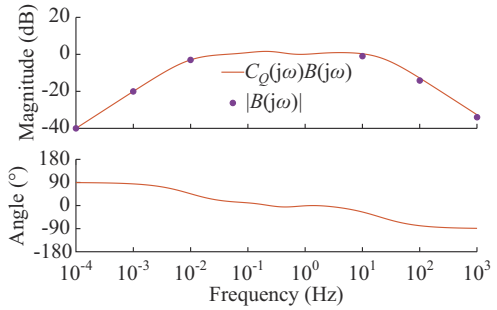

Fig. 7. Frequency response of $C_Q(s)B(s)$ and magnitude of $B(\mathrm{j}\omega)$ for all elements in Ω_{out}.

C. Controller Gain

Figure 8 shows the system frequency response for modified gain values of K_P and K_Q. Here, the system is in nominal configuration, with all its lines connected. It can be ob-

served that the increase of the proportional gain has a two-fold effect on the system dynamic property. First, for three low-frequency peaks, the system magnitude decreases as the gain value increases. At the same time, the change in the opposite direction is observed for peaks outside the frequency range of interest, shown as gray areas in Fig. 8. Thus, the system stability margins for frequencies outside the range of low-frequency oscillation, are reduced with an increase of the controller gains. These results show the importance of analyzing stability margins for frequencies within and outside the frequency range of interest. Based on this analysis, the proportional gains are set to be $K_P = K_Q = 1.3$. These values, together with the rest of the relevant system parameters, are summarized in Table SBI of Supplementary Material B. Figure SB3 of Supplementary Material B shows the comparison of the system transient responses after a disturbance is applied.

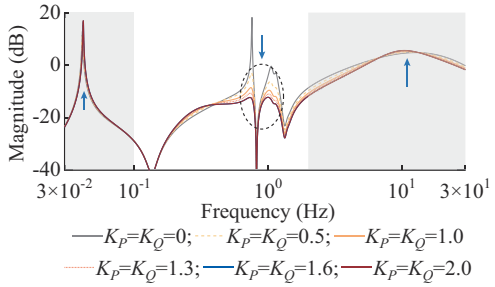

Fig. 8. System frequency response for modified gain values of K_P and K_Q.

Figure 9 shows the most relevant system eigenvalues for different network configurations without POD controller, with a standard POD controller and the proposed POD controller. Darker marks are used to represent the system eigenvalues for the nominal network configuration. The eigenvalue analysis covers the eigenvalues in the range of low-frequency oscillations, i.e., from 0.1 Hz to 2 Hz. However, for improving readability, Fig. 9 shows the eigenvalues in a more narrow frequency range and with real parts above −3 rad/s. Also, all critical eigenvalues are included in the plotted range.

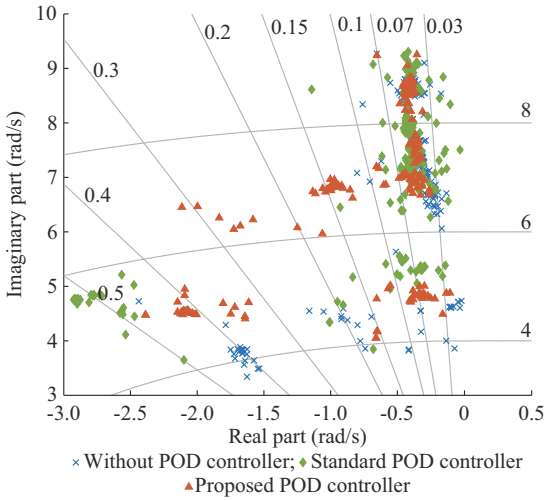

Fig. 9. Most relevant system eigenvalues for different network topologies.

Several conclusions can be drawn by comparing the results. First, the introduction of either a standard or the proposed POD controller improves the damping of the system eigenvalues in the majority of the cases. However, it can be observed that in certain cases, the standard POD controller makes the system unstable, since it is designed by considering only the nominal network configuration. Therefore, the impact on the system is unknown when the network topology changes. Second, the proposed POD controller does not cause system instability for any of the network configurations. This result highlights the importance of addressing the network reconfiguration during the design stage of the proposed POD controllers.

D. Performance Under Unconsidered Changes

The proposed method for the design of the proposed POD controller addresses the changes in the network topology, caused by the disconnection of any single line at a time. However, during the operation, the system conditions may change in different ways. For example, the system loading level is constantly changing. Also, the total inertia in the system can vary depending on the level of conventional generation and CIG-based power plants in operation. Furthermore, the disconnection of generation units in the system may occur, causing significant changes in the system dynamics. Figure 10 shows the system eigenvalues for those changes applied to the system with the proposed POD controller. The analysis of these results is presented as follows.

1) Changes of Inertia

In Fig. 10(a), the most relevant system eigenvalues are presented when the inertia of all generators is reduced to 90% and 80% of its nominal value. In each test case, the lines in the power system are disconnected, one at a time. The results show that, when the inertia is reduced, the natural frequency of the eigenvalues is reduced significantly, while the damping ratio is marginally changed. Moreover, the groups of eigenvalues from different network topologies follow the same pattern. Also, as the inertia is reduced, the groups of eigenvalues are moving further apart, which means that the disconnection of lines has more impact on the system with reduced inertia. These results uniformly show that the reduction of the inertia has an important impact on the system frequency stability in the range of low-frequency oscillations. However, even with 20% less inertia in the system, the system remains stable for all network configurations, which shows the robustness of the proposed POD controller even against those changes that are not originally considered.

2) Changes of Loading Level

In Fig. 10(b), the relevant eigenvalues for three levels of load consumption are presented when one line is disconnected at a time. In all the cases, the proposed POD controller is connected. It can be observed that the load reduction does not affect all the system modes in the same way. In most cases, the load reduction increases the natural frequency and reduces the damping factor of the system modes. However, for certain modes, the same load reduction reduces the natural frequencies. Therefore, it can be concluded that the load

level affects the low-frequency modes in different ways. Nonetheless, the system remains stable for all the network topologies, even under 30% load reduction, highlighting that the proposed design method produces controllers that are robust even against cases that are not considered in the design procedure.

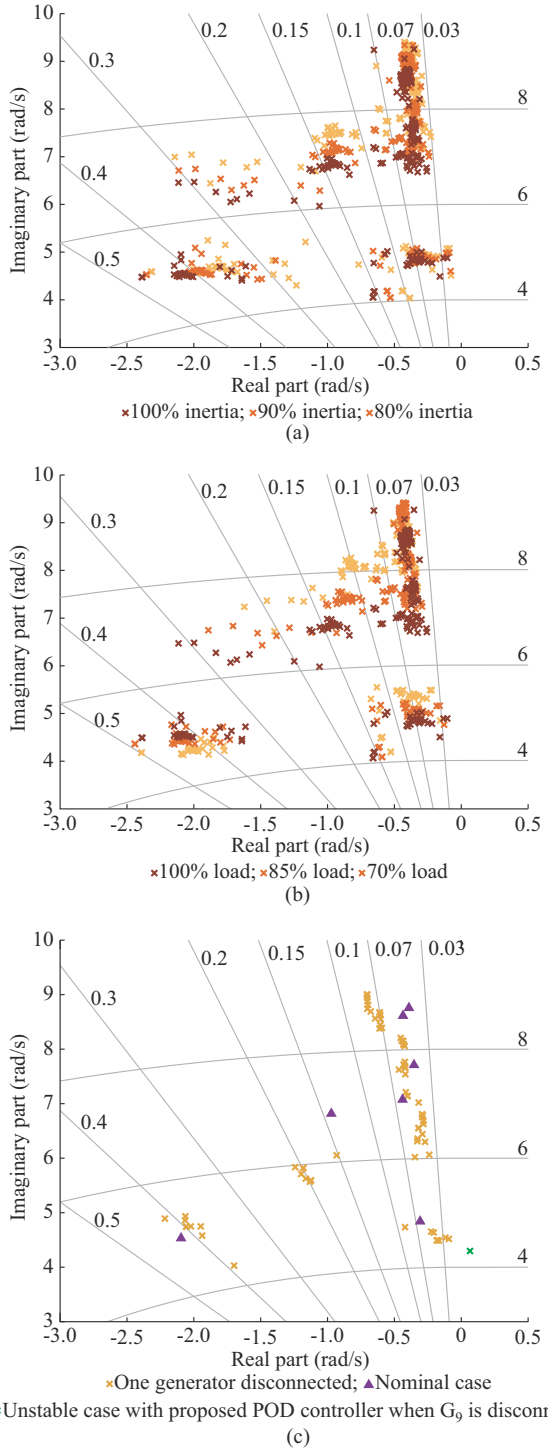

Fig. 10. Eigenvalues for different cases. (a) Eigenvalues for different network topologies when proposed POD controller is active (with three levels of inertia). (b) Eigenvalues for different network topologies when proposed POD controller is active (with three levels of loads). (c) Eigenvalues when proposed POD controller is applied in nominal case with one generator disconnected.

3) Disconnection of Generators

Figure 10(c) shows the eigenvalues when the proposed POD controller is applied in nominal case with one generator disconnected. In the nominal case, the system is stable and the damping factor is always above 0.05. In the rest of the cases, one generator from G_2-G_{10} is disconnected at a time. G_1 has not been disconnected as it is represented as an equivalent representation of a large system [30]. It can be observed that the eigenvalues become less damped when one generator is disconnected. The results show that the system remains stable in most of the cases, except when G_9 is disconnected. It should be noted that the disconnection of generators is not included in the optimization problem, therefore, this result could be expected. Nonetheless, the disconnection of generators is a relevant problem and the proposed method could be extended to include those cases in the design of the proposed POD controllers.

Supplementary Material C includes a discussion on several aspects related to the design methodology for the proposed POD controllers. The content is briefly described here. First, the coordinated design of multiple POD controllers in different CIG-based generator is presented. Then, the effect of system partitioning is described and alternative methods to deal with large variations in the power plant is summarized. Finally, the impact of weak grids in the controller performance is addressed.

VI. Conclusion

The contributions presented in this paper are as follows.

1) A method for designing the proposed POD controller for CIG-based power plants is introduced. The design procedure considers the changes in the system caused by network reconfiguration.

2) It has been explained that how all the necessary information for the proposed method is obtained from the system frequency response. An optimization-based design procedure for the proposed POD controller has been introduced.

3) The formulation of the optimization problem including all the system constraints has been proposed and its objective is defined.

All the steps of the design procedure and its validation have been explained in detail. The proposed method is tested using the IEEE 39-bus system [34] by disconnecting one transmission line per test case. The proposed method is useful for applications in which a small-signal model of the power system is not available but there is a simulation model. However, the small-signal model of the IEEE 39-bus system [38] is used to analyze the impact of the proposed POD controller on the system, i.e., for eigenvalue analysis.

Once the proposed POD controller is introduced, the changes in the network topology have limited impact on the margins of the critical eigenvalues. It has been shown that the resilience of the controller against network reconfiguration increases with the number of lead-lag filter stages, although the controller performance barely increases after a certain number of stages. Also, the results have demonstrated that the system eigenvalues remain well-damped for all the possible cases, highlighting the principal advantage of

the design of the proposed POD controller.

Future work can focus on studying the performance of the proposed design method applied to different networks because the relation between the oscillation frequency and the compensation angles depends on the network topology. Furthermore, the application of the proposed design method for CIG operation in the grid-forming mode can be studied. The comparison of the performance of CIG operation in grid-forming and grid-following modes with the designed POD controller could be conducted.

REFERENCES

[1] P. Kundur, N. Balu, and M. Lauby, *Power System Stability and Control*. New York: McGraw-Hill, 1994.

[2] IEEE PES Energy Development and Power Generation Committee, "IEEE recommended practice for excitation system models for power system stability studies," IEEE PES, Tech. Rep., 2005.

[3] R. Shah, N. Mithulananthan, and R. Bansal, "Oscillatory stability analysis with high penetrations of large-scale photovoltaic generation," *Energy Conversion and Management*, vol. 65, pp. 420-429, Jan. 2013.

[4] International Energy Agency. (2018, Jan.). Total primary energy supply (TPES) by source, year and country. [Online]. Available: https://www.iea.org/data-and-statistics

[5] *Technical Norm of Supervision on Electrical Generation Modules*, EU Regulation 2016/631, 2019.

[6] Transpower New Zealand, "Normal frequency management strategy," Transpower New Zealand, Tech. Rep., 2019.

[7] E. V. Larsen and D. A. Swann, "Applying power system stabilizers: part I: general concepts," *IEEE Transactions on Power Apparatus and Systems*, vol. 100, no. 6, pp. 3017-3024, Jun. 1981.

[8] H. Geng, X. Xi, L. Liu *et al*., "Hybrid modulated active damping control for DFIG-based wind farm participating in frequency response," *IEEE Transactions on Energy Conversion*, vol. 32, no. 3, pp. 1220-1230, Sept. 2017.

[9] P. Sun, J. Yao, Y. Zhao *et al*., "Stability assessment and damping optimization control of multiple grid-connected virtual synchronous generators," *IEEE Transactions on Energy Conversion*, vol. 36, no. 4, pp. 3555-3567, Dec. 2021.

[10] M. Basu, V. R. Mahindara, J. Kim *et al*., "Comparison of active and reactive power oscillation damping with PV plants," *IEEE Transactions on Industry Applications*, vol. 57, no. 3, pp. 2178-2186, May 2021.

[11] D. Rimorov, I. Kamwa, and G. Joos, "Coordinated design of active and reactive power modulation auxiliary loops of wind turbine generators for oscillation damping in power systems," in *Proceedings of 2015 IEEE PES General Meeting*, Denver, USA, Oct. 2015, pp. 1-5.

[12] S. Yang, R. Shen, J. Shu *et al*., "PLL based sub-/super-synchronous resonance damping controller for D-PMSG wind farm integrated power systems," *IEEE Transactions on Energy Conversion*, vol. 37, no. 4, pp. 2370-2384, Dec. 2022.

[13] Y. Zhu, C. Liu, B. Wang *et al*., "Damping control for a target oscillation mode using battery energy storage," *Journal of Modern Power Systems and Clean Energy*, vol. 6, no. 4, pp. 833-845, Jul. 2018.

[14] N. Jankovic, J. Roldán-Pérez, M. Prodanovic *et al*., "Power oscillation damping method suitable for network reconfigurations based on converter interfaced generation and combined use of active and reactive powers," *International Journal of Electrical Power & Energy Systems*, vol. 149, p. 109010, Jul. 2023.

[15] T. K. Chau, S. Yu, T. Fernando *et al*., "A load-forecasting-based adaptive parameter optimization strategy of STATCOM using ANNs for enhancement of LFOD in power systems," *IEEE Transactions on Industrial Informatics*, vol. 14, no. 6, pp. 2463-2472, Jun. 2018.

[16] W. Yao, L. Jiang, J. Fang *et al*., "Adaptive power oscillation damping controller of superconducting magnetic energy storage device for inter-area oscillations in power system," *International Journal of Electrical Power & Energy Systems*, vol. 78, pp. 555-562, Jun. 2016.

[17] J. Arif, S. Ray, and B. Chaudhuri, "Multivariable self-tuning feedback linearization controller for power oscillation damping," *IEEE Transactions on Control Systems Technology*, vol. 22, no. 4, pp. 1519-1526, Jul. 2014.

[18] J. Deng, J. Suo, J. Yang *et al*., "Adaptive damping control strategy of wind integrated power system," *Energies*, vol. 12, no. 1, pp. 1-18, Jan. 2019.

[19] G. Zhang, W. Hu, D. Cao *et al*., "A novel deep reinforcement learning enabled sparsity promoting adaptive control method to improve the stability of power systems with wind energy penetration," *Renewable Energy*, vol. 178, pp. 363-376, Nov. 2021.

[20] A. I. Konara and U. D. Annakkage, "Robust power system stabilizer design using Eigenstructure assignment," *IEEE Transactions on Power Systems*, vol. 31, no. 3, pp. 1845-1853, May 2016.

[21] H. Werner, P. Korba, and T. Yang, "Robust tuning of power system stabilizers using LMI-techniques," *IEEE Transactions on Control Systems Technology*, vol. 11, no. 1, pp. 147-152, Jan. 2003.

[22] D. Sambariya and R. Prasad, "Robust tuning of power system stabilizer for small signal stability enhancement using metaheuristic bat algorithm," *International Journal of Electrical Power & Energy Systems*, vol. 61, pp. 229-238, Oct. 2014.

[23] D. Chitara, K. R. Niazi, A. Swarnkar *et al*., "Cuckoo search optimization algorithm for designing of a multimachine power system stabilizer," *IEEE Transactions on Industry Applications*, vol. 54, no. 4, pp. 3056-3065, Jul. 2018.

[24] N. Gupta and S. Narayan, "Design of power system stabilizer using robust control techniques," in *Proceedings of 2015 International Conference on Recent Developments in Control, Automation and Power Engineering (RDCAPE)*, Noida, India, Oct. 2015, pp. 66-71.

[25] P. Chaubey, J. Lather, S. Yelisetti *et al*., "Robust power system stabilizer based on static output feedback approach to enhance power system stability," *Energy Procedia*, vol. 158, pp. 2960-2965, Feb. 2019.

[26] H. M. Soliman and K. A. El Metwally, "Robust pole placement for power systems using two-dimensional membership fuzzy constrained controllers," *IET Generation, Transmission & Distribution*, vol. 11, no. 16, pp. 3966-3973, Aug. 2017.

[27] R. Shah, N. Mithulananthan, and K. Y. Lee, "Low-order robust damping controller design for large-scale PV power plants," in *Proceedings of IEEE PES General Meeting*, National Harbor, USA, Oct. 2014, pp. 1-5.

[28] G. Zhang, J. Zhao, W. Hu *et al*., "Deep reinforcement learning enabled bi-level robust parameter optimization of hydropower-dominated systems for damping ultra-low frequency oscillation," *Journal of Modern Power Systems and Clean Energy*, vol. 11, no. 6, pp. 1770-1783, Nov. 2023.

[29] C. Yuan and X. Yan, "Multi-objective robust tuning of STATCOM controller parameters for stability enhancement of stochastic wind-penetrated power systems," *IET Generation, Transmission & Distribution*, vol. 14, pp. 4805-4814, Sept. 2020.

[30] IEEE PES Task Force on Benchmark Systems for Stability Controls, "Benchmark systems for small-signal stability analysis and control," IEEE, Tech. Rep., 2015.

[31] A. Yazdani and R. Iravani, *Grid-Imposed Frequency VSC System: Control in dq-Frame*. New York: John Wiley & Sons, 2010, pp. 160-203.

[32] M. Klein, G. Rogers, and P. Kundur, "A fundamental study of inter-area oscillations in power systems," *IEEE Transactions on Power Systems*, vol. 6, no. 3, pp. 914-921, Aug. 1991.

[33] J. Zhao, A. Gómez-Expósito, M. Netto *et al*., "Power system dynamic state estimation: motivations, definitions, methodologies, and future work," *IEEE Transactions on Power Systems*, vol. 34, no. 4, pp. 3188-3198, Jul. 2019.

[34] MATLAB, *Version 9.7.0 (R2019b)*. Natick: The MathWorks Inc., 2019.

[35] R. G. Lyons, *Understanding Digital Signal Processing.* Noida: Pearson Education India, 2004.

[36] K. Ogata, *Modern Control Engineering*. Upper Saddle River: Prentice Hall, 2010.

[37] N. Jankovic, J. Roldán-Pérez, and M. Prodanovic, "Power oscillation damping using converter-interfaced generators under constrained active and reactive powers," in *Proceedings of 2021 IEEE PES Innovative Smart Grid Technologies Europe*, Espoo, Finland, Oct. 2021, pp. 1-8.

[38] B. Patrice. (2016, Jan.). 10-machine new-England power system IEEE benchmark. [Online]. Available: https://www. mathworks. com/matlabcentral/fileexchange/54771-10-machine-new-england-power-system-ieee-benchmark.

Njegos Jankovic received the B. Sc. and M. Eng. degrees in electrical and computer engineering from the Faculty of Technical Science, University of Novi Sad, Novi Sad, Serbia, in 2016 and 2017, respectively. In 2024, he received the Ph.D. degree in power system stability from Comillas Pontificial

University, Madrid, Spain. From 2017 to 2019, he was with Typhoon HIL company, Serbia, developing models of electrical elements. From 2019 to 2023, he was with IMDEA Energy Institute, Madrid, Spain, where he worked as a Pre-doctoral Researcher. In 2022, he was with SINTEF Energy AS Institute, Trondheim, Norway, as a Visiting Researcher. From 2023 to 2024, he has been with the Power Engineering Department at SepsaMedha as a Control Engineer. Since October 2024, he is with Mjolner Informatics, as a Control Engineer in the domain of wind turbines. His research interests include power system stability analysis, integration of renewable energy source, and control of power electronic device.

Javier Roldán-Pérez received the B.S. degree in industrial engineering, the M.S. degree in electronics and control systems, the M.S. degree in system modeling, and the Ph.D. degree in power electronics, all from Comillas Pontifical University, Madrid, Spain, in 2009, 2010, 2011, and 2015, respectively. From 2010 to 2015, he was with the Institute for Research in Technology, Comillas University, Madrid, Spain. In 2014, he was a Visiting Ph.D. Student at the Department of Energy Technology, Aalborg University, Aalborg, Denmark. From 2015 to 2016, he was with the Electric and Control Systems Department at Norvento Energia Distribuida, Valencia, Spain. In September 2016, he joined the Electrical Systems Unit at IMDEA Energy Institute, Madrid, Spain. In 2018, he did a research stay at SINTEF Energy Research, Trondheim, Norway. His research interests include integration of renewable energy, microgrid, and power electronic application.

Milan Prodanovic received the B.Sc. degree in electrical engineering from the University of Belgrade, Belgrade, Serbia, in 1996, and the Ph.D. degree in electric and electronic engineering from Imperial College, London, U.K., in 2004. From 1997 to 1999, he was with GVS engineering company, Serbia, developing uninterruptible power supply systems. From 1999 until 2010, he was a Research Associate in electrical and electronic engineering with Imperial College. He is currently a Senior Researcher and Head of the Electrical Systems Unit, Institute IMDEA Energy, Madrid, Spain. His research interests include design and control of power electronic interface for distributed generation, microgrid stability and control, and active management of distribution network.

Jon Are Suul received the M.Sc. degree in energy and environmental engineering and the Ph.D. degree in electric power engineering from the Norwegian University of Science and Technology (NTNU), Trondheim, Norway, in 2006 and 2012, respectively. From 2006 to 2007, he was with the SINTEF Energy Research, until starting his Ph.D. studies. Since 2012, he resumed a position as a Research Scientist at the SINTEF Energy Research, first in part-time while also working as a Postdoctoral Researcher in the Department of Electric Power Engineering, NTNU, until 2016. His research interests include modeling, analysis, and control of power electronic converter in power system and for renewable energy application.

Salvatore D'Arco received the M.Sc. and Ph.D. degrees in electrical engineering from the University of Naples "Federico II", Naples, Italy, in 2002 and 2005, respectively. From 2006 to 2007, he was a Postdoctoral Researcher at the University of South Carolina, Columbia, USA. In 2008, he joined ASML, Veldhoven, The Netherlands, as a Power Electronics Designer, where he worked until 2010. From 2010 to 2012, he was a Postdoctoral Researcher in the Department of Electric Power Engineering, Norwegian University of Science and Technology, Trondheim, Norway. In 2012, he joined the SINTEF Energy Research, Trondheim, Norway, where he is currently a Research Scientist. His research interests include control and analysis of power electronic conversion system for power system application, including real-time simulation and rapid prototyping of converter control system.

Luis Rouco obtained the M.Sc. and Ph.D. degrees from Comillas Pontificial University, Madrid, Spain, in 1985 and 1990, respectively. He is a Full Professor of the School of Engineering (ICAI) of Comillas Pontificial University attached to the Department of Electrical Engineering. He develops his research activities at the Instituto de Investigación Tecnológica (IIT), ICAI, Universidad Pontificia Comillas. He is a Distinguished Member of CIGRE where he convenes the Advisory Group on Wind Generation and New Technologies of Study Committee A1 on Rotating Machines. He has been Visiting Engineer at MIT, Ontario Hydro, and ABB Power Systems. His research interests include modeling, analysis, and simulation of power system.